
Electronic Supplementary Information

Anion-Specific Aggregation Induced Phosphorescence Emission (AIPE) in an Ionic Iridium Complex in Aqueous Media

Guangfu Li,^{‡a} Wei Guan,^{‡a} Shuang Du,^b Dongxia Zhu,^{a*} Guogang Shan,^a Xiaojuan Zhu,^b Likai Yan,^a Zhongmin Su,^{a*} Martin R. Bryce^{c*} and Andrew P. Monkman^d

^a*Institute of Functional Material Chemistry, Faculty of Chemistry, Northeast Normal*

University, Changchun 130024, P. R. China; Fax: +86-0431-85684009

Tel.: +86-431-85099108, E-mail: zhudx047@nenu.edu.cn; zmsu@nenu.edu.cn

^b*Key Laboratory of Molecular Epigenetics of the Ministry of Education, Institute of Cytology and Genetics,*

Northeast Normal University, Renmin Street No. 5268, Changchun, 130024, P. R. China

E-mail: zhuxj720@nenu.edu.cn

^c*Department of Chemistry, Durham University, Durham, DH1 3LE, UK*

E-mail: m.r.bryce@durham.ac.uk

^d*Department of Physics, Durham University, Durham, DH1 3LE, UK*

E-mail: a.p.monkman@durham.ac.uk

Table of Contents

1. Experimental - general information
2. Photophysical properties
3. Dynamic light scattering (DLS) experiments
4. ¹⁹F NMR spectra and MALDI-TOF negative-ion mass spectrometry
5. Quantum chemical calculations
6. ¹H NMR, ¹³C NMR, 2D NMR spectra of complexes **1**•2PF₆ and **1**•2ClO₄ at room temperature
7. X-ray crystallographic data
8. Supporting information references

1. Experimental - general information

Materials obtained from commercial suppliers were used without further purification unless otherwise stated. All glassware, syringes, magnetic stirring bars, and needles were thoroughly dried in a convection oven. Reactions were monitored using thin layer chromatography (TLC). Commercial TLC plates were used and the spots were visualised under UV light at 254 and 365 nm. ^1H NMR, ^{13}C NMR, ^{19}F NMR and 2D ^1H NMR spectra were recorded at 25 °C on a Varian 500 MHz spectrometer; ^{13}C NMR spectra were recorded at 25 °C on a Varian 125 MHz, and TMS as internal standard. The chemical shifts (δ) are given in parts per million relative to internal standard TMS (0 ppm for ^1H) and DMSO- d_6 (40.0 ppm for ^{13}C). The molecular weights of the complexes were obtained by using matrix-assisted laser desorption-ionization time-of-flight (MALDI-TOF) mass spectrometry. Elemental analysis was obtained using a Flash EA1112 analyser. UV-vis absorption spectra were recorded on a Shimadzu UV-3100 spectrophotometer. Photoluminescence spectra were collected on a Shimadzu RF-5301PC spectrophotometer and Maya 2000Pro optical fiber spectrophotometer. PL efficiencies were measured with an integrating sphere (C-701, Labsphere Inc.), with a 365 nm Ocean Optics LLS-LED as the excitation source, and the laser was introduced into the sphere through the optical fiber. The excited-state lifetimes were measured by exciting the samples with 355 nm light pulses with ~ 3 ns pulse width from a Quanta-Ray DCR-2 pulsed Nd:YAG laser. DLS measurements were conducted on a Malvern Zetasizer Nano-ZS instrument. Transmission electron microscopy (TEM) was performed using a TECNAI F20 microscope. Fluorescence microscopy images were taken on Nikon-80i inverted fluorescence microscope. Crystal structure data for complexes $\mathbf{1}\cdot 2\text{PF}_6$ and $\mathbf{1}\cdot 2\text{ClO}_4$ were collected on a Bruker Smart Apex II CCD diffractometer with graphite-monochromated Mo $K\alpha$ radiation ($\lambda = 0.71073 \text{ \AA}$) at room temperature.

 Complexes **1**•2PF₆ and **1**•2ClO₄ - synthesis and characterisation

 Synthesis of [(2Cl-ppz)₂Ir-(L)-Ir(2Cl-ppz)₂] [PF₆]₂ (complex **1**•2PF₆)

A yellow suspension of the dichloro-bridged diiridium complex [Ir(2Cl-ppz)₂Cl]₂¹ (0.100 g, 0.1 mmol, 1.00 eq.) and bridging ligand (L) (0.029 g, 0.1 mmol, 1.00 eq.) in MeOH (15 mL) and CH₂Cl₂ (15 mL) was refluxed under an inert atmosphere of N₂ in the dark for 4 h. The orange solution was then cooled to room temperature and solid ammonium hexafluorophosphate (0.055 g, 0.3 mmol, 3.00 eq.) was added to the solution. The mixture was stirred for 45 min at room temperature and the suspension was then filtered and the precipitate was washed with petroleum ether and dried. The crude product was recrystallized from petroleum ether to yield complex **1**•2PF₆ as an orange solid (0.121 g, 67% yield). Complex **1**•2PF₆ exists in solution as a pair of diastereoisomers. There is a slight excess of one isomer over the other (ca. 1.23:1). The major isomer is arbitrarily designated as α (*cis*-conformation); the minor as β (*trans*-conformation). Where separate signals are visible for the two isomers, they are reported separately, but in each case integrals are quoted relative to the molecular formula for that isomer (i.e. 1H represents one hydrogen for that isomer). ¹H NMR (500 MHz, DMSO-d₆, δ [ppm]): 9.33 (s, 1H, H^{A β}), 9.31 (s, 1H, H^{A α}), 9.30 (d, $J = 5.0$ Hz, 1H, H^{E 6β}), 9.29 (d, $J = 6.0$ Hz, 1H, H^{E 6α}), 9.17 (d, 1H, $J = 6.0$ Hz, H^{B 3β}), 9.16 (d, $J = 5.0$ Hz, 1H, H^{B 3α}), 8.51 (d, $J = 9.0$ Hz, 2H, H^{E $3\alpha+\beta$}), 8.35 (t, $J = 8.0$ Hz, 2H, H^{E $4\alpha+\beta$}), 8.01 (d, $J = 7.0$ Hz, 2H, H^{D $3\alpha+\beta$}), 7.88 (d, $J = 5.0$ Hz, 1H, H^{B 5α}), 7.80-7.76 (m, 3H, H^{B 5β +D $5\alpha+\beta$}), 7.58 (s, 1H, H^{A 4β}), 7.51 (s, 1H, H^{A 4α}), 7.35 (s, 1H, H^{A 6α}), 7.28 (s, 1H, H^{A 6β}), 7.27 (s, 1H, H^{C 6β}), 7.23 (s, 1H, H^{C 6α}), 7.04 (t, $J = 6.0$ Hz, 1H, H^{B 4α}), 7.01 (t, $J = 6.0$ Hz, 1H, H^{B 4β}), 6.98 (t, $J = 6.0$ Hz, 1H, H^{D 4β}), 6.91 (t, $J = 6.0$ Hz, 1H, H^{D 4α}), 6.71 (d, $J = 5.0$ Hz, 4H, H^{F $2\alpha+\beta$}), 5.89 (s, 1H, H^{C 4α}), 5.79 (s, 1H, H^{C 4β}), 5.63 (t, $J = 5.0$ Hz, 2H, H^{E $5\alpha+\beta$}). ¹³C NMR (DMSO-d₆, 125 MHz, δ [ppm]): 109.9(C^{D $4\alpha+\beta$}), 110.1(C^{B $4\alpha+\beta$}), 117.7(C^{C $1\alpha+\beta$}), 118.1(C^{A $1\alpha+\beta$}), 123.0(C^{F $2\alpha+\beta$}), 125.1(C^{A $6\alpha+\beta$}), 125.9(C^{C $6\alpha+\beta$}), 130.3(C^{C $5\alpha+\beta$}), 130.5(C^{A 5α}), 130.6(C^{C 4β}), 130.8(C^{C 4α}), 130.9(C^{E $5\alpha+\beta$}), 131.0(C^{A 5β}), 131.3(C^{D $5\alpha+\beta$}), 131.9(C^{E $3\alpha+\beta$}), 134.0(C^{B $3\alpha+\beta$}), 134.2(C^{E $6\alpha+\beta$}), 136.5(C^{A $3\alpha+\beta$}), 138.0(C^{C $3\alpha+\beta$}), 138.2(C^{F $1\alpha+\beta$}), 138.4(C^{E 2α}), 138.6(C^{E 2β}), 140.8(C^{E $4\alpha+\beta$}), 141.2(C^{B 5β}),

141.3(C^{A4α}), 141.5(C^{A4β}), 141.7(C^{B5α}), 147.7(C^{C2α}), 147.8(C^{C2β}), 151.5(C^{D3α}), 151.6(C^{D3β}), 155.6(C^{A2α}), 155.7(C^{A2β}), 172.4(C^{aα}), 172.5(C^{aβ}). MS: (MALDI-TOF) [m/z]: 1805.89 (M-PF₆) (calcd: 1805.91). Anal. Calcd. for C₅₄H₃₄Cl₈F₁₂Ir₂N₁₂P₂: C 37.85, H 1.89, N 9.29. Found C 37.84, H 1.91, N 9.28. Crystals for X-ray analysis were obtained by slow evaporation of an acetonitrile-water solution of the complex.

Synthesis of [(2Cl-ppz)₂Ir-(L)-Ir(2Cl-ppz)₂] [ClO₄]₂ (complex **1**•2ClO₄)

The synthesis of complex **1**•2ClO₄ was similar to that of complex **1**•2PF₆ except that the counter anion PF₆⁻ was replaced by ClO₄⁻. Complex **1**•2ClO₄ was obtained as a yellow solid (0.131 g, 76% yield). Complex **1**•2ClO₄ exists in solution as a pair of diastereoisomers with an isomeric ratio of ca. 2.58:1. The major isomer is arbitrarily designated as α (*cis*-conformation); the minor as β (*trans*-conformation). Where separate signals are visible for the two isomers, they are reported separately, but in each case integrals are quoted relative to the molecular formula for that isomer (i.e. 1H represents one hydrogen for that isomer). ¹H NMR (500 MHz, DMSO-d₆, δ [ppm]): 9.33 (s, 1H, H^{aβ}), 9.31 (s, 1H, H^{aα}), 9.30 (d, *J* = 5.0 Hz, 1H, H^{E6β}), 9.29 (d, *J* = 6.0 Hz, 1H, H^{E6α}), 9.17 (d, 1H, *J* = 6.0 Hz, H^{B3β}), 9.16 (d, *J* = 5.0 Hz, 1H, H^{B3α}), 8.51 (d, *J* = 9.0 Hz, 2H, H^{E3α+β}), 8.35 (t, *J* = 8.0 Hz, 2H, H^{E4α+β}), 8.01 (d, *J* = 7.0 Hz, 2H, H^{D3α+β}), 7.88 (d, *J* = 5.0 Hz, 1H, H^{B5α}), 7.80-7.76 (m, 3H, H^{B5β+D5α+β}), 7.58 (s, 1H, H^{A4β}), 7.51 (s, 1H, H^{A4α}), 7.35 (s, 1H, H^{A6α}), 7.28 (s, 1H, H^{A6β}), 7.27 (s, 1H, H^{C6β}), 7.23 (s, 1H, H^{C6α}), 7.04 (t, *J* = 6.0 Hz, 1H, H^{B4α}), 7.01 (t, *J* = 6.0 Hz, 1H, H^{B4β}), 6.98 (t, *J* = 6.0 Hz, 1H, H^{D4β}), 6.91 (t, *J* = 6.0 Hz, 1H, H^{D4α}), 6.71 (d, *J* = 5.0 Hz, 4H, H^{F2α+β}), 5.89 (s, 1H, H^{C4α}), 5.79 (s, 1H, H^{C4β}), 5.63 (t, *J* = 5.0 Hz, 2H, H^{E5α+β}). ¹³C NMR (DMSO-d₆, 125 MHz, δ [ppm]): 109.9(C^{D4α+β}), 110.1(C^{B4α+β}), 117.7(C^{C1α+β}), 118.1(C^{A1α+β}), 123.0(C^{F2α+β}), 125.1(C^{A6α+β}), 125.9(C^{C6α+β}), 130.3(C^{C5α+β}), 130.5(C^{A5α}), 130.6(C^{C4β}), 130.8(C^{C4α}), 130.9(C^{E5α+β}), 131.0(C^{A5β}), 131.3(C^{D5α+β}), 131.9(C^{E3α+β}), 134.0(C^{B3α+β}), 134.2(C^{E6α+β}), 136.5(C^{A3α+β}), 138.0(C^{C3α+β}), 138.2(C^{F1α+β}), 138.4(C^{E2α}), 138.6(C^{E2β}), 140.8(C^{E4α+β}), 141.2(C^{B5β}), 141.3(C^{A4α}), 141.5(C^{A4β}), 141.7(C^{B5α}), 147.7(C^{C2α}), 147.8(C^{C2β}), 151.5(C^{D3α}), 151.6(C^{D3β}), 155.6(C^{A2α}), 155.7(C^{A2β}), 172.4(C^{aα}), 172.5(C^{aβ}). MS: (MALDI-TOF) [m/z]: 1717.87

(M-PF₆) (calcd: 1713.88). Anal. Calcd. for C₅₄H₃₄Cl₁₀Ir₂N₁₂O₈: C 37.75, H 1.99, N 9.78. Found C 37.74, H 1.97, N 9.79.

[(2Cl-ppz)₂Ir-(L)-Ir(2Cl-ppz)₂] [ClO₄]₂ (complex **1**•2ClO₄: *cis*-conformation)

Complex 1•2ClO₄ was recrystallized from hot dichloromethane. The solid which did not dissolve was collected by filtration of the hot dichloromethane to yield **1**•2ClO₄ (*cis*-conformation) (0.095 g, 72%). ¹H NMR (500 MHz, DMSO-d₆, δ [ppm]): 9.30-9.29 (m, 2H, H^{a+E6}), 9.16 (d, 1H, *J* = 6.0 Hz, H^{B3}), 8.51 (d, *J* = 9.0 Hz, 1H, H^{E3}), 8.36 (t, *J* = 8.0 Hz, 1H, H^{E4}), 7.99 (d, *J* = 7.0 Hz, 1H, H^{D3}), 7.86 (d, *J* = 5.0 Hz, 1H, H^{B5}), 7.77 (d, 1H, H^{D5}), 7.50 (s, 1H, H^{A4}), 7.42 (s, 1H, H^{A6}), 7.32 (s, 1H, H^{C6}), 7.04 (t, *J* = 5.0 Hz, 1H, H^{B4}), 6.90 (t, *J* = 5.0 Hz, 1H, H^{D4}), 6.70 (d, *J* = 5.0 Hz, 2H, H^{F2}), 5.88 (s, 1H, H^{C4}), 5.61 (t, *J* = 5.0 Hz, 1H, H^{E5}). Crystals for X-ray analysis were obtained by the slow diffusion of ether vapor into a solution of the complex in acetonitrile solution, with slow evaporation of the solvent mixture.

[(2Cl-ppz)₂Ir-(L)-Ir(2Cl-ppz)₂] [ClO₄]₂ (complex **1**•2ClO₄: *trans*-conformation)

Complex 1•2ClO₄ was recrystallised from hot dichloromethane. The dichloromethane filtrate was evaporated in vacuo to afford **complex 1**•2ClO₄ (*trans*-conformation) (0.036 g, 28%). ¹H NMR (500 MHz, DMSO-d₆, δ [ppm]): 9.31-9.29 (m, 2H, H^{a+E6}), 9.25 (d, 1H, *J* = 6.0 Hz, H^{B3}), 8.51 (d, *J* = 9.0 Hz, 1H, H^{E3}), 8.34 (t, *J* = 8.0 Hz, 1H, H^{E4}), 8.01 (d, *J* = 7.0 Hz, 1H, H^{D3}), 7.79-7.75 (m, 2H, H^{B5+D5}), 7.58 (s, 1H, H^{A4}), 7.39 (s, 1H, H^{A6}), 7.37 (s, 1H, H^{C6}), 7.01 (t, *J* = 5.0 Hz, 1H, H^{B4}), 6.98 (t, *J* = 5.0 Hz, 1H, H^{D4}), 6.70 (d, *J* = 5.0 Hz, 2H, H^{F2}), 5.78 (s, 1H, H^{C4}), 5.60 (t, *J* = 5.0 Hz, 1H, H^{E5}). Crystals for X-ray analysis were obtained by the slow diffusion of ether vapour into a solution of the complex in acetonitrile solution, with slow evaporation of the solvent mixture.

2. Photophysical properties

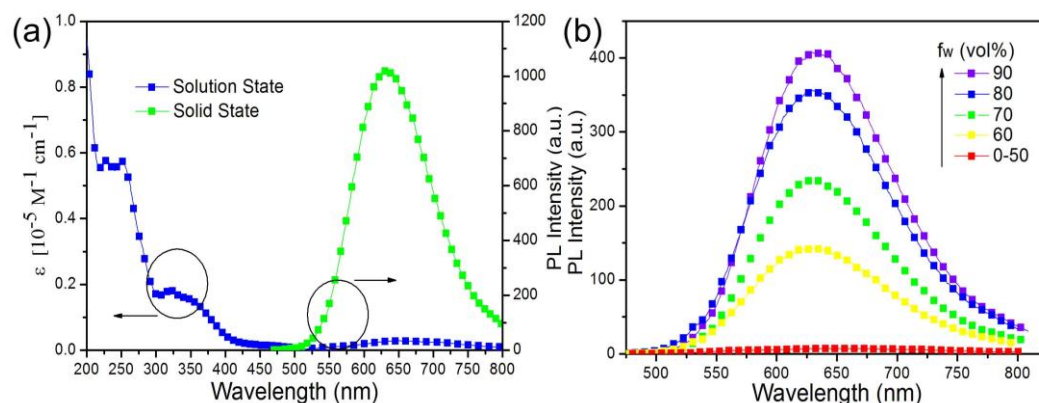


Fig. S1 (a) UV-Vis absorption and emission spectra of complex **1•2PF₆** (1.0×10^{-5} M) in degassed CH₃CN solution and solid state at room temperature; (b) Emission spectra of complex **1•2PF₆** in CH₃CN–H₂O mixtures with different water fractions (0–90%).

Table S1 Photophysical and electrochemical characteristics of complexes **1•2PF₆**, *cis*-**1•2ClO₄** and *trans*-**1•2ClO₄**.

	Absorption and emission at room temperature			Emission at 77 K	Electrochemical Data ^d		K_r $\times 10^6 \text{ s}^{-1}$	K_{nr} $\times 10^6 \text{ s}^{-1}$
	λ_{abs}^a (nm)	λ_{em}^b (nm)	Φ_{em}^b (τ^b [μs])	λ_{em}^c (nm)	$E_{\text{ox}}^{1/2}$ (V)	$E_{\text{red}}^{1/2}$ (V)		
1•2PF₆	249(0.581), 352 _{sh} (0.167)	613	0.17(0.17)	562	0.63	-1.49	1.00	4.88
1•2ClO₄	251(0.874), 366 _{sh} (0.203)	602	0.26(0.24)	558	0.65	-1.49	1.08	3.08
<i>cis</i> - 1•2ClO₄	253(0.754), 367 _{sh} (0.188)	601	0.31(0.25)	557	0.65	-1.49	1.24	2.76
<i>trans</i> - 1•2ClO₄	253(0.762), 368 _{sh} (0.192)	602	0.13(0.18)	561	0.64	-1.50	0.72	4.83

^aMeasured in CH₂Cl₂ (1.0×10^{-5} M). ^bMeasured in solid state ($\lambda_{\text{exc}} = 365$ nm; error for $\Phi_L \pm 5\%$). ^cIn CH₃CN glass. ^dThe data are versus Fc⁺/Fc (Fc is ferrocene).

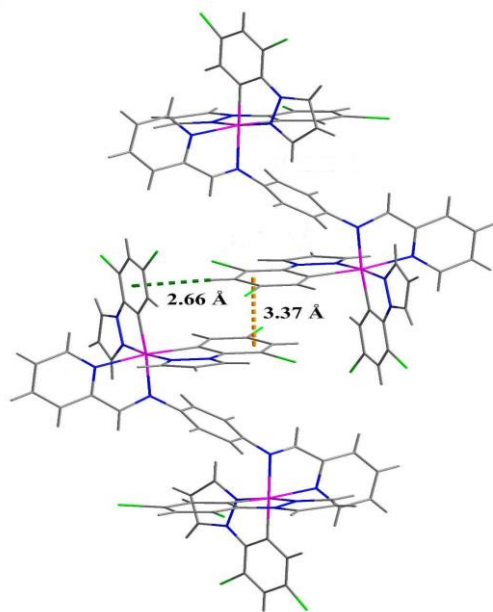


Fig. S2 Interactions between two molecules of complex **1•2PF₆** in the crystal structure. Anions are omitted for clarity.

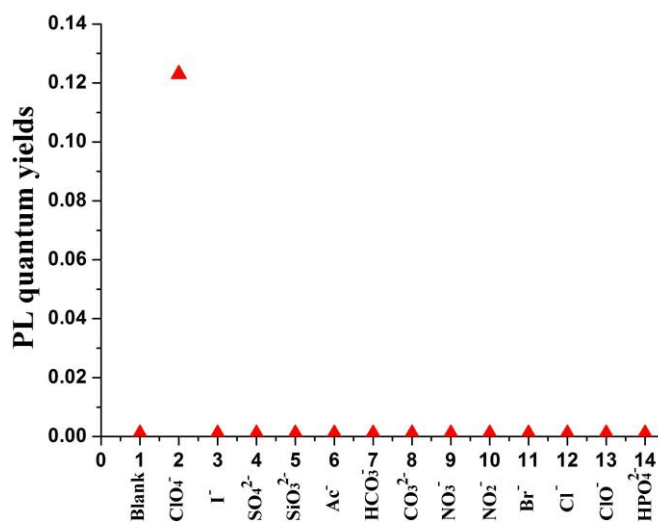


Fig. S3 PL quantum yields of complex **1•2PF₆** (10 μM) in the presence of different anions (1 - PF₆⁻ (blank), 2 - ClO₄⁻, 3 - I⁻, 4 - SO₄²⁻, 5 - SiO₃²⁻, 6 - Ac⁻, 7 - HCO₃⁻, 8 - CO₃²⁻, 9 - NO₃⁻, 10 - NO₂⁻, 11 - Br⁻, 12 - Cl⁻, 13 - ClO⁻, 14 - HPO₄²⁻) (15 equiv.) in 10 mM HEPES buffer (pH = 7.4) (CH₃CN/water, 1:4, v/v), excited at 365 nm.

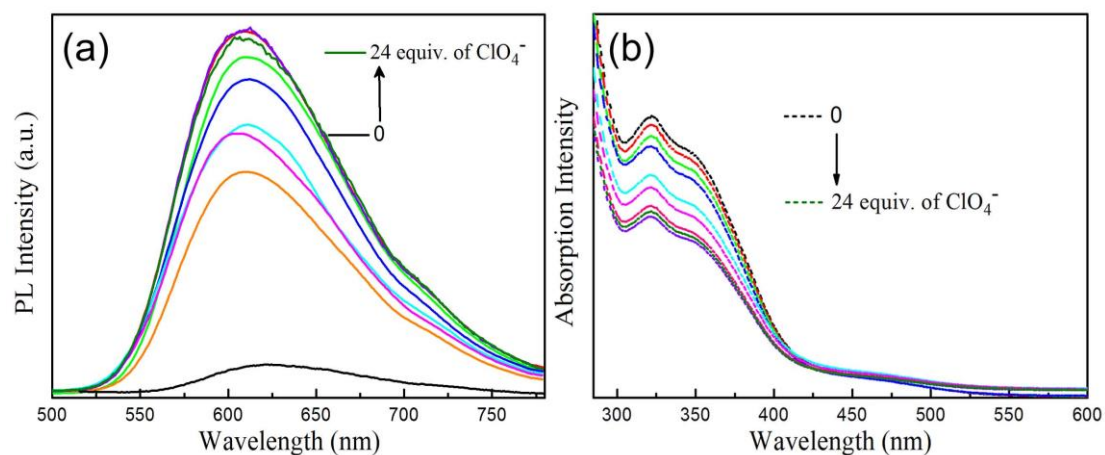


Fig. S4 (a) Phosphorescence spectra of complex $1 \cdot 2PF_6$ (10 μM) upon addition of different amounts of ClO_4^- anion (0, 20, 30, 60, 90, 120, 150, 180, 240 μM), in HEPES buffer (CH_3CN /water, 1:4, v/v), excited at 365 nm. A similar excess of counterions has been used in previous work.² (b) The corresponding absorption spectra.

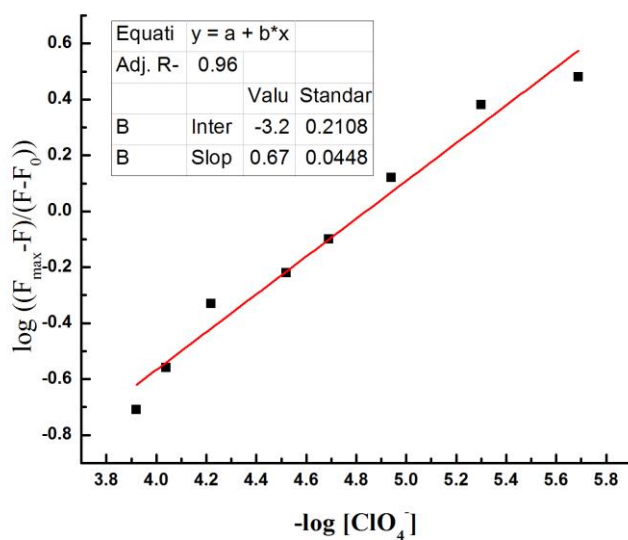


Fig. S5 Hill plot from the spectrophotometric titration (phosphorescence intensity of $1 \cdot 2PF_6$ at 602 nm was used).

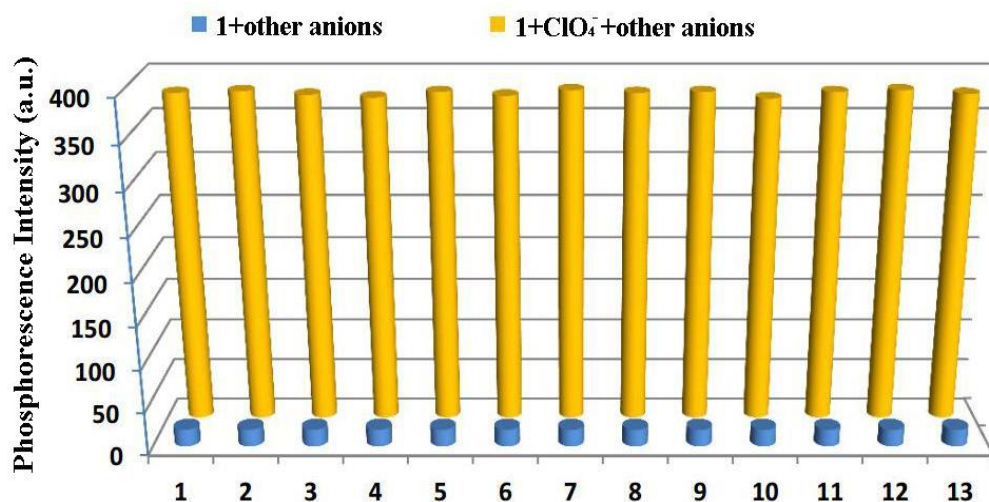


Fig. S6 Plot of the emission intensity of complex $1 \cdot 2\text{ClO}_4$ system in the presence of different anions: complex $1 \cdot 2\text{PF}_6$ ($10 \mu\text{M}$) + ClO_4^- ($150 \mu\text{M}$) + other anions ($150 \mu\text{M}$), where other anions = (1 - I^- , 2 - SO_4^{2-} , 3 - SiO_3^{2-} , 4 - Ac^- , 5 - HCO_3^- , 6 - CO_3^{2-} , 7 - NO_3^- , 8 - HPO_4^{2-} , 9 - Br^- , 10 - ClO^- , 11 - Mix. (solutions of I^- , SO_4^{2-} , SiO_3^{2-} , Ac^- , HPO_4^{2-}), 12 - Mix. (solutions of HCO_3^- , CO_3^{2-} , NO_3^- , ClO^-), 13 - Mixture (solutions of NO_2^- , Br^- , Cl^-) in HEPES buffer (10 mM , $\text{CH}_3\text{CN}:\text{H}_2\text{O}$, 1:4, v/v).

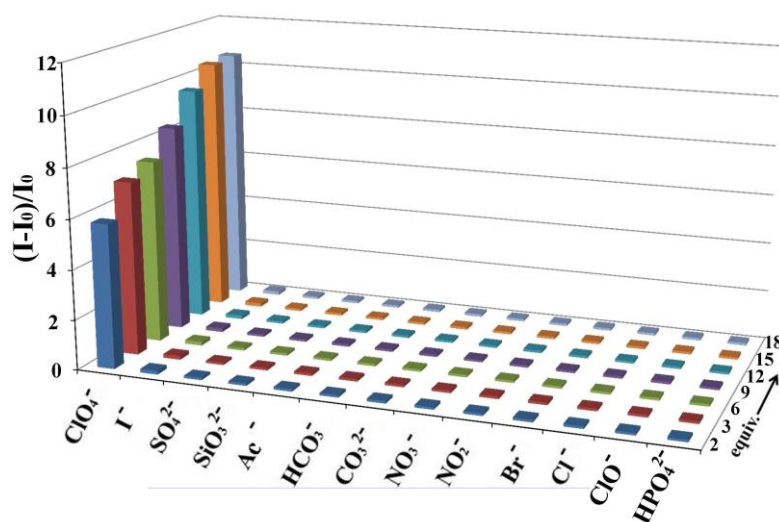


Fig. S7 Emission enhanced efficiency of complex $1 \cdot 2\text{PF}_6$ in HEPES buffer ($\text{CH}_3\text{CN}/\text{water}$, 1:4, v/v).

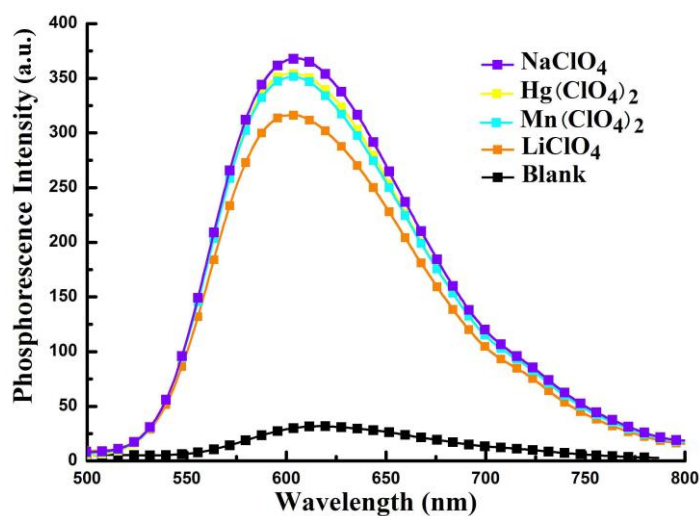


Fig. S8 Phosphorescence spectra of complex **1•2PF₆** (10 μ M) in the presence of different cations (Na^+ , Li^+ , Hg^{2+} , Mn^{2+}) (15 equiv.) in 10 mM HEPES buffer (pH = 7.4) ($\text{CH}_3\text{CN}/\text{water}$, 1:4, v/v).

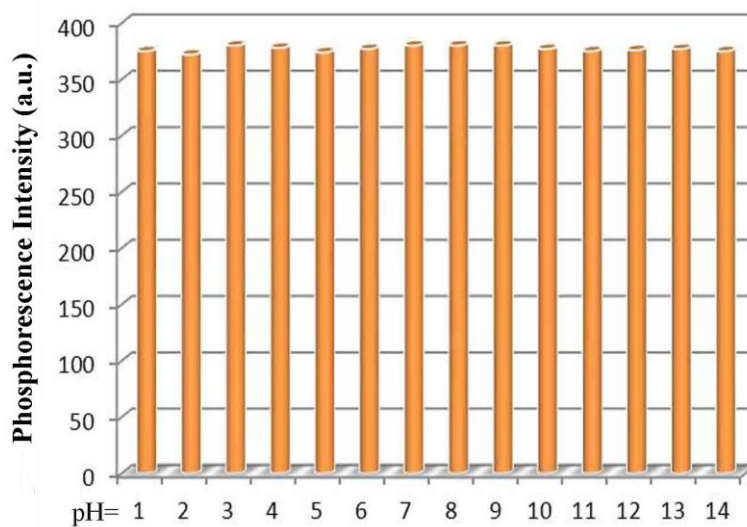


Fig. S9 The effect of pH on the emission intensity of complex **1•2PF₆** (10 μ M) in $\text{CH}_3\text{CN}/\text{water}$ (1:4, v/v) system containing 15 equiv. ClO_4^- .

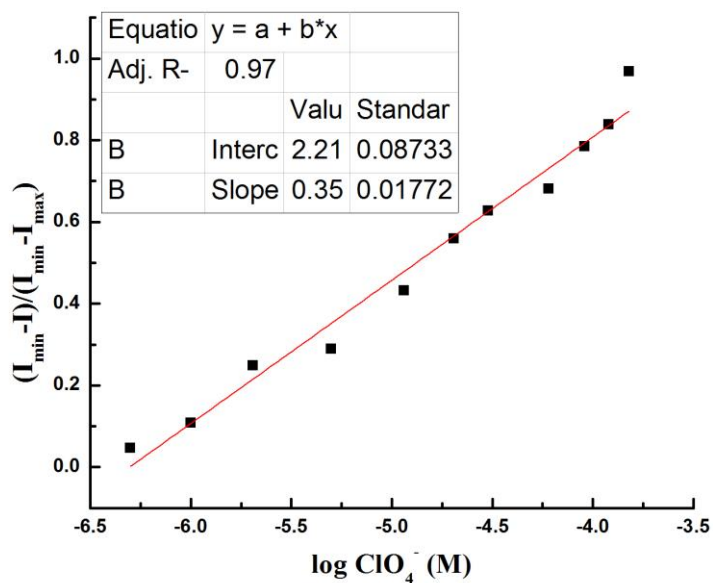


Fig. S10 Estimation of ClO_4^- (0–150 μM) with $1 \cdot 2\text{PF}_6$ (10 μM) by means of normalized phosphorescence intensity ($I_{\min} - I / I_{\min} - I_{\max}$) at $\lambda_{\max} = 603$ nm in HEPES buffer ($\text{CH}_3\text{CN}/\text{water}$, 1:4, v/v).

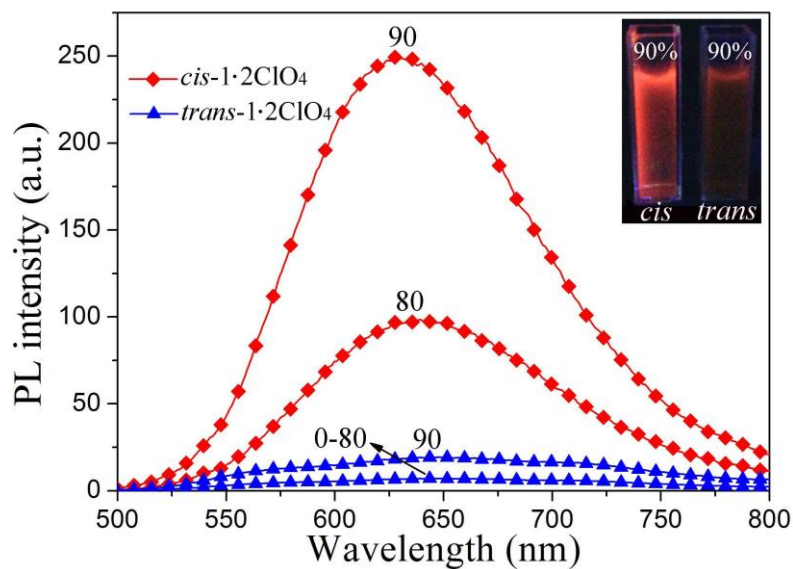


Fig. S11 Emission spectra of *cis*- $1 \cdot 2\text{ClO}_4$ and *trans*- $1 \cdot 2\text{ClO}_4$ (2×10^{-5} M) in CH_3CN –water mixtures with different water fractions (0–90% v/v).

3. Dynamic light scattering (DLS) experiments

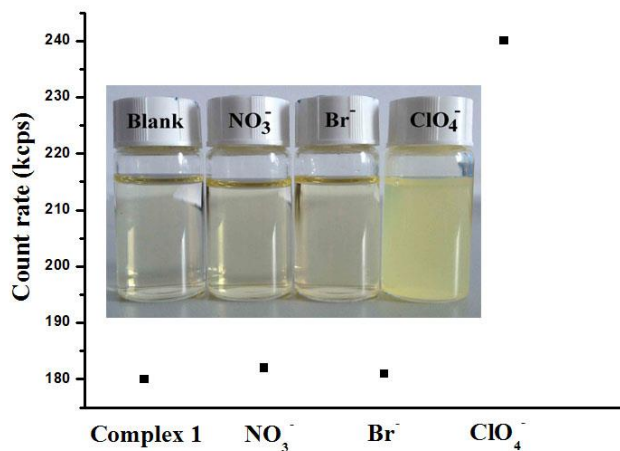


Fig. S12 The count rate (from left to right): complex $1 \cdot 2\text{PF}_6$ ($10 \mu\text{M}$), complex $1 \cdot 2\text{PF}_6$ with 15 equiv. of NO_3^- ions, complex $1 \cdot 2\text{PF}_6$ with 15 equiv. of Br^- ions, complex $1 \cdot 2\text{PF}_6$ with 15 equiv. of ClO_4^- ions, all in $\text{CH}_3\text{CN}/\text{H}_2\text{O}$ (1:4, v/v) at 25°C .

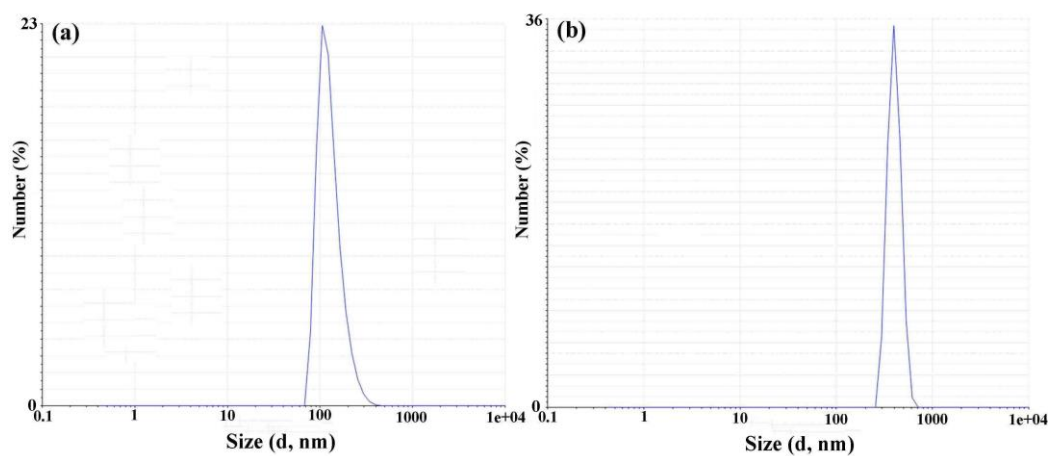


Fig. S13 DLS profile of complex $1 \cdot 2\text{PF}_6$ ($10 \mu\text{M}$) in $\text{CH}_3\text{CN}/\text{H}_2\text{O}$ (1:4, v/v) (a) before and (b) after addition of ClO_4^- (15 equiv.).

4. ^{19}F NMR spectra and MALDI-TOF negative-ion mass spectrometry

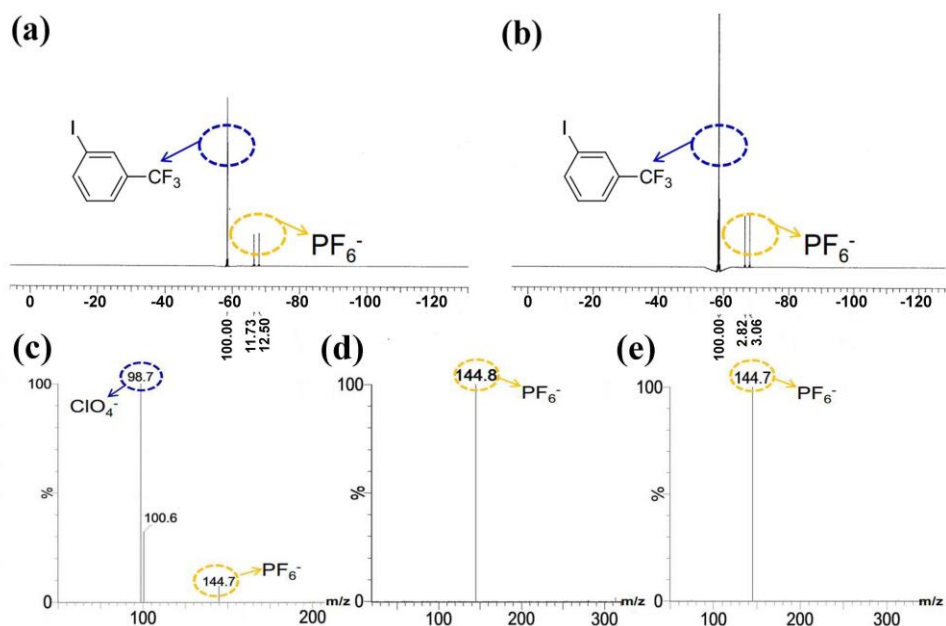


Fig. S14 ^{19}F NMR spectrum of **1**• 2PF_6 (a) before PF_6^- exchange by ClO_4^- (internal standard = 1-iodo-3-(trifluoromethyl)benzene); (b) after PF_6^- anion exchange by ClO_4^- . MALDI-TOF MS spectrum of complex **1**• 2PF_6 (negative mode) with addition of different anions, (15 equiv.) (c) ClO_4^- ; (d) Br^- ; (e) NO_3^- .

5. Quantum chemical calculations

AIPE mechanism. The B3LYP functional^{3,4} was employed for these calculations. The 6-31G* basis set was used for the H, C, N and Cl atoms. The Ir atom was described by Los Alamos relativistic effective core potentials (ECPs) and double- ξ basis set LANL2DZ.⁵ Full geometry optimizations with C_1 symmetry constraints were carried out in solution for the singlet ground state (S_0) and triplet excited state (T_1) of complex $\mathbf{1}\cdot 2\text{PF}_6$. A solvent effect was taken into account by the polarizable continuum model (PCM) with acetonitrile as solvent.⁶ In addition, single point calculations were performed using the crystal structure of complex $\mathbf{1}\cdot 2\text{PF}_6$ at the same level.

Anion-capturing ability. These geometry optimizations were performed using the M06 functional.⁷ The LANL2DZ basis set was employed for the Ir atom with Los Alamos relativistic ECPs,⁵ while the 6-31G* basis set was used for the other main-group elements. The solvent effect of toluene was evaluated by the conductor-like polarizable continuum model (CPCM).^{6,8,9}

All the calculations were carried out with the Gaussian 09 program.¹⁰

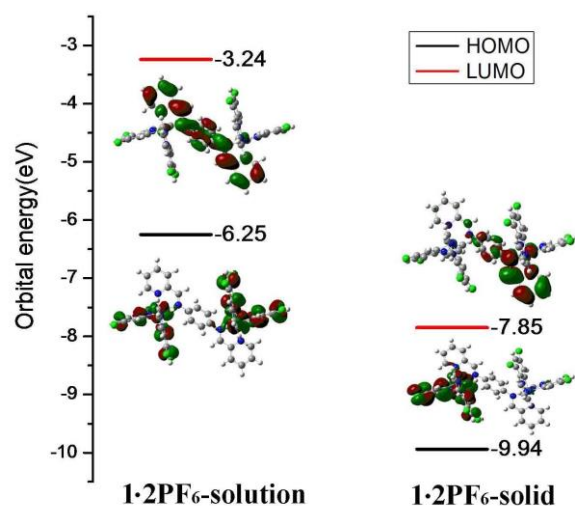


Fig. S15 Molecular orbital diagrams, HOMO and LUMO energies for complex $\mathbf{1}\cdot 2\text{PF}_6$ at its S_0 optimized geometries in solution and in the solid state.

Table S2 Selected calculated bond lengths (Å), bond angles (°) and dihedral angles (°) at both optimized S_0 and T_1 geometries for complex **1**• $2PF_6$ in acetonitrile solution. The atom numbering is shown in Figure S22.

	S_0	T_1
Ir1-C32	2.024	2.022
Ir1-C23	2.028	2.031
Ir1-N5	2.042	2.041
Ir1-N7	2.046	2.046
Ir1-N1	2.243	2.267
Ir1-N2	2.204	2.202
Ir2-C50	2.029	2.030
Ir2-C41	2.025	2.028
Ir2-N9	2.045	2.042
Ir2-N11	2.043	2.038
Ir2-N3	2.234	2.223
Ir2-N4	2.202	2.204
C32-Ir1-C23	88.32	87.65
C32-Ir1-N5	95.36	95.38
C23-Ir1-N1	100.51	102.04
N1-Ir1-N5	90.95	91.70
C32-Ir1-N2	96.25	95.63
N1-Ir1-N2	75.24	75.13
C32-Ir1-N1	170.00	168.95
N2-Ir1-C23	174.27	174.53
N5-Ir1-N7	172.64	172.70
C41-Ir2-C50	88.29	86.82
C50-Ir2-N11	79.06	79.14
C41-Ir2-N3	171.87	168.91
N3-Ir2-N11	87.06	88.20
C50-Ir2-N4	173.69	176.81
N3-Ir2-N4	75.35	76.45
C50-Ir2-N3	99.61	104.12
N4-Ir2-C41	96.88	92.73
N9-Ir2-N11	173.71	173.63
C7-N1-C1-C6	-48.33	-38.28
C13-N3-C4-C3	45.99	16.47

Table S3 The reaction energy for anion-capturing (ΔE , in kcal mol⁻¹) calculated at the M06/[6-31G*/LANL2DZ(Ir)] and CPCM(acetonitrile)/M06/[6-31G*/LANL2DZ(Ir)] levels.

entry	anion	model reaction	ΔE	
			gas	acetonitrile
1	ClO ₄ ⁻	<i>trans</i> (1 •2PF ₆) + 2NaClO ₄ → <i>trans</i> (1 •2ClO ₄) + 2NaPF ₆	-10.1	-8.6
2	ClO ⁻	<i>trans</i> (1 •2PF ₆) + 2NaClO → <i>trans</i> (1 •2ClO) + 2NaPF ₆	5.6	12.3
3	Br ⁻	<i>trans</i> (1 •2PF ₆) + 2NaBr → <i>trans</i> (1 •2Br) + 2NaPF ₆	0.3	8.9
4	Cl ⁻	<i>trans</i> (1 •2PF ₆) + 2NaCl → <i>trans</i> (1 •2Cl) + 2NaPF ₆	3.8	13.3
5	Ac ⁻	<i>trans</i> (1 •2PF ₆) + 2NaAc → <i>trans</i> (1 •2Ac) + 2NaPF ₆	25.1	18.2
6	NO ₃ ⁻	<i>trans</i> (1 •2PF ₆) + 2NaNO ₃ → <i>trans</i> (1 •2NO ₃) + 2NaPF ₆	5.6	8.6
7	HCO ₃ ⁻	<i>trans</i> (1 •2PF ₆) + 2NaHCO ₃ → <i>trans</i> (1 •2HCO ₃) + 2NaPF ₆	21.4	16.3
8	NO ₂ ⁻	<i>trans</i> (1 •2PF ₆) + 2NaNO ₂ → <i>trans</i> (1 •2NO ₂) + 2NaPF ₆	19.7	18.4
9	CO ₃ ²⁻	<i>trans</i> (1 •2PF ₆) + Na ₂ CO ₃ → <i>trans</i> (1 •CO ₃) + 2NaPF ₆	26.0	15.2
10	SO ₄ ²⁻	<i>trans</i> (1 •2PF ₆) + Na ₂ SO ₄ → <i>trans</i> (1 •SO ₄) + 2NaPF ₆	27.5	20.2
11	SiO ₃ ²⁻	<i>trans</i> (1 •2PF ₆) + Na ₂ SiO ₃ → <i>trans</i> (1 •SiO ₃) + 2NaPF ₆	27.9	11.9
12	HPO ₄ ²⁻	<i>trans</i> (1 •2PF ₆) + Na ₂ HPO ₄ → <i>trans</i> (1 •HPO ₄) + 2NaPF ₆	30.2	20.1

6. ^1H NMR, ^{13}C NMR, 2D NMR spectra of complexes $1\cdot 2\text{PF}_6$ and $1\cdot 2\text{ClO}_4$ at room temperature

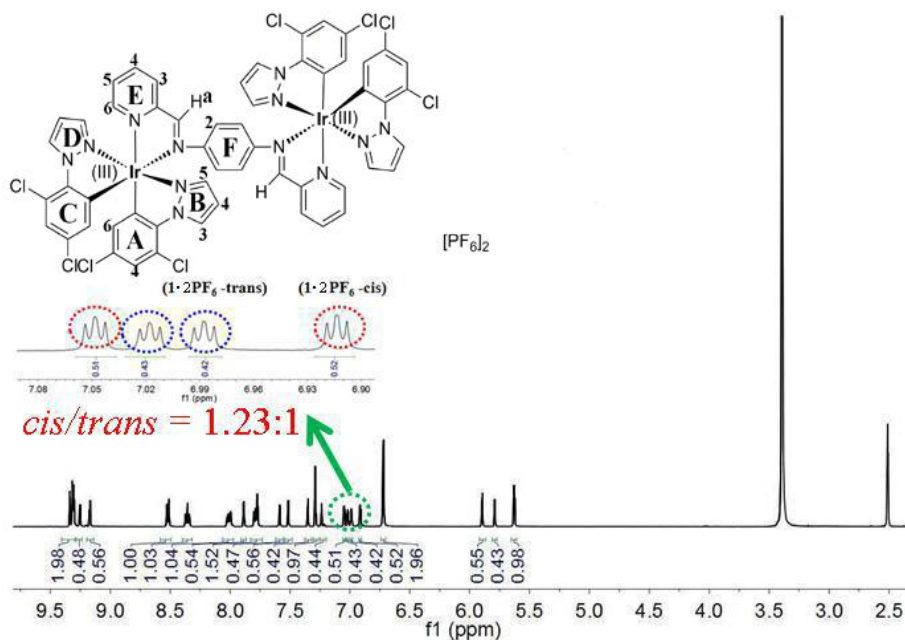


Fig. S16 ^1H NMR spectrum of complex $1\cdot 2\text{PF}_6$ in DMSO-d_6 , inset: expansion of two pairs of *cis-trans* isomer peaks in the range from 6.90-7.06 ppm.

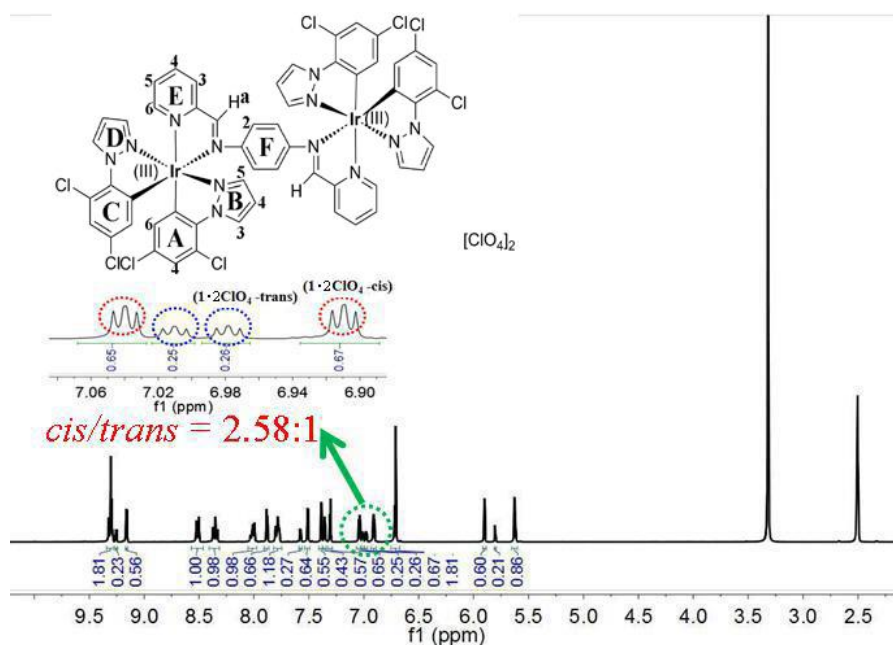


Fig. S17 ^1H NMR spectrum of complex $1\cdot 2\text{ClO}_4$ in DMSO-d_6 , inset: expansion of two pairs of *cis-trans* isomer peaks in the range from 6.90-7.06 ppm.

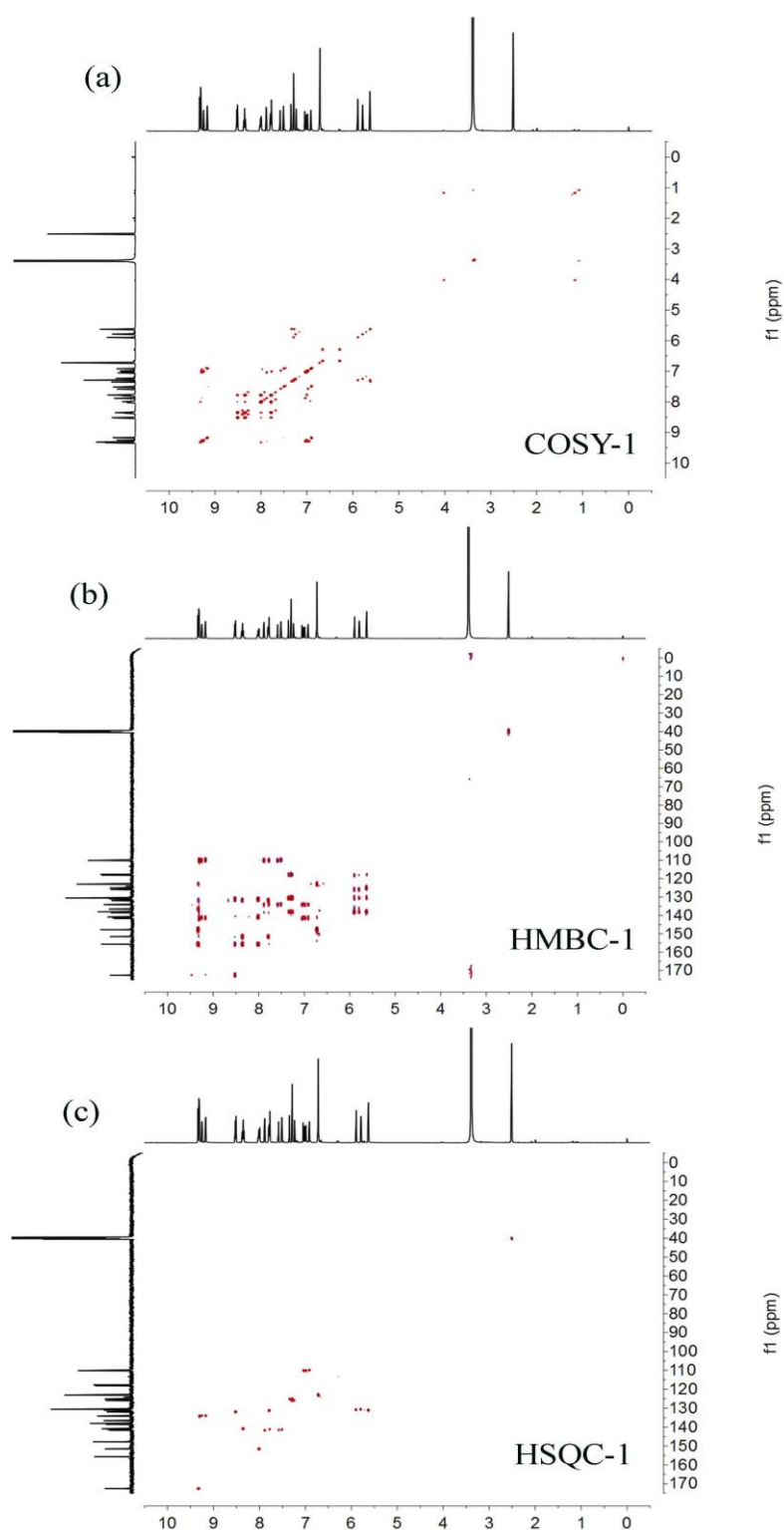


Fig. S18 (a) 2D COSY NMR spectrum of complex $\mathbf{1}\cdot\mathbf{2PF}_6$ in DMSO- d_6 ; (b) 2D HMBC NMR spectrum of complex $\mathbf{1}\cdot\mathbf{2PF}_6$ in DMSO- d_6 ; (c) 2D HSQC NMR spectrum of complex $\mathbf{1}\cdot\mathbf{2PF}_6$ in DMSO- d_6 .

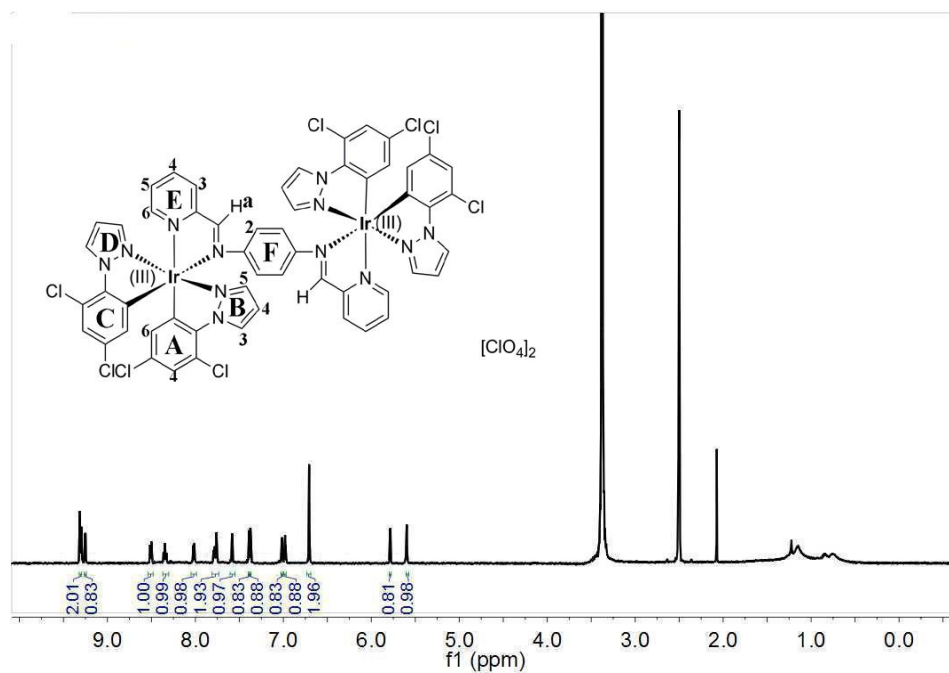


Fig. S19 ^1H NMR spectrum of complex **1**• 2ClO_4 (*trans*-conformation) in DMSO-d_6 .

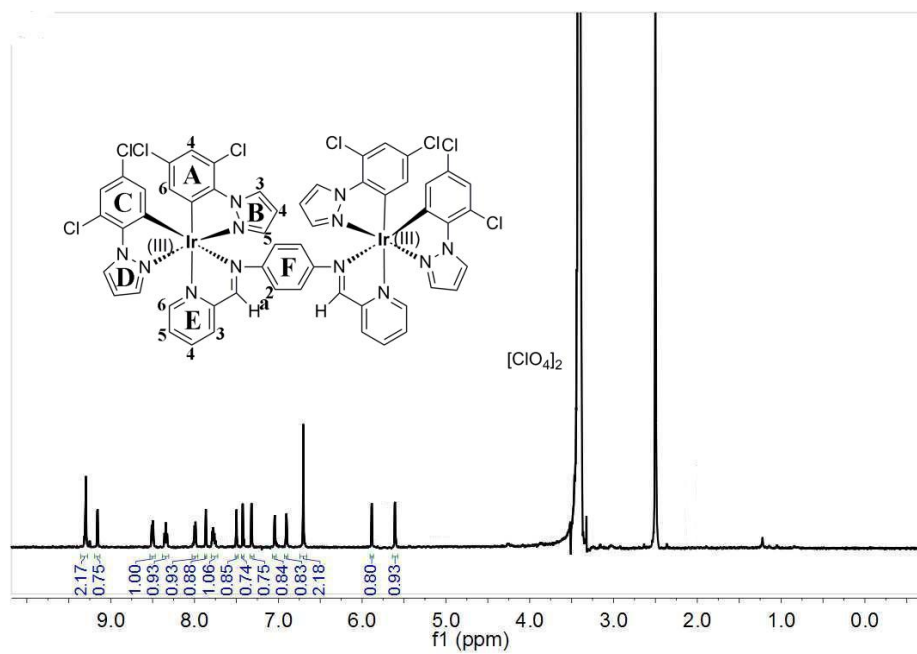


Fig. S20 ^1H NMR spectrum of complex **1**• 2ClO_4 (*cis*-conformation) in DMSO-d_6 .

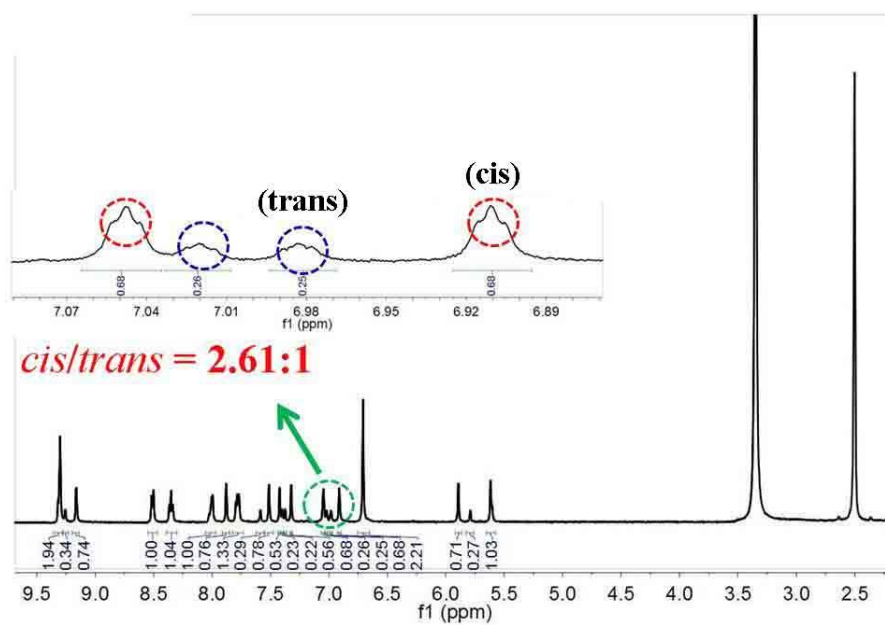


Fig. S21 ^1H NMR titration experiments of $\mathbf{1}\cdot 2\text{PF}_6$ with ClO_4^- in HEPES buffer ($\text{CH}_3\text{CN}/\text{water}$, 1:4, v/v), inset: expansion of two pairs of *cis-trans* isomer peaks in the range from 6.89-7.07 ppm.

7. X-ray crystallographic data

The molecular structures of complexes $\mathbf{1}\cdot 2\text{PF}_6$, $\mathbf{1}\cdot 2\text{ClO}_4$ (*cis*-conformation) and $\mathbf{1}\cdot 2\text{ClO}_4$ (*trans*-conformation) were confirmed by X-ray crystallographic analysis of single crystals. Diffraction data were collected on a Bruker SMART Apex CCD diffractometer using $k(\text{Mo-K})$ radiation ($k = 0.71073 \text{ \AA}$). Cell refinement and data reduction were made by the SAINT program. The structure was determined using the SHELXTL/PC program. Fig. 4 shows Oak Ridge thermal ellipsoid plot (ORTEP) drawings of complexes *trans*- $\mathbf{1}\cdot 2\text{PF}_6$, *cis*- $\mathbf{1}\cdot 2\text{ClO}_4$ and *trans*- $\mathbf{1}\cdot 2\text{ClO}_4$. The crystallographic data have been deposited with the Cambridge Crystallographic Data Centre with CCDC deposition numbers 1043904, 1043944 and 1043946. These data can be obtained free of charge from The Cambridge Crystallographic Data Centre via www.ccdc.cam.ac.uk/data_request/cif.

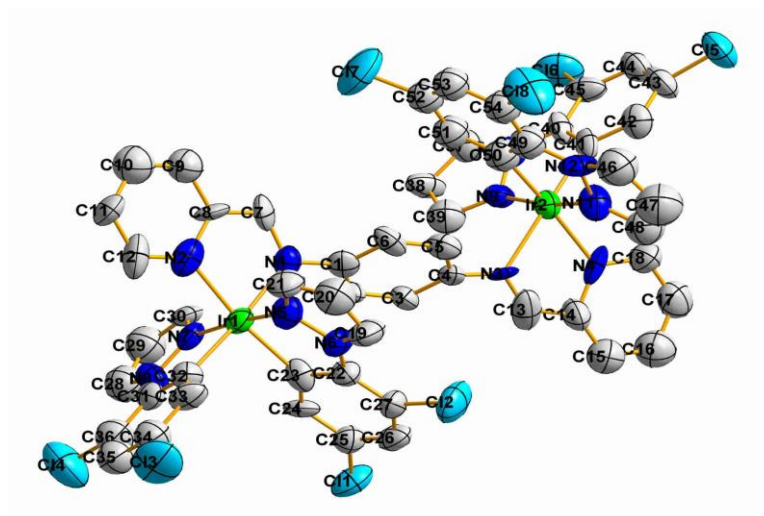


Fig. S22 The dication in the molecular structures of *trans*- $\mathbf{1}\cdot 2\text{PF}_6$ in the crystal. The H atoms, PF_6^- anions and solvent molecules are omitted for clarity. This atom numbering scheme is used in Table S2.

Table S4 Crystal data and structure refinement for *trans*-**1**•2PF₆, *cis*-**1**•2ClO₄ and *trans*-**1**•2ClO₄.

	<i>trans</i> - 1 •2PF ₆	<i>cis</i> - 1 •2ClO ₄	<i>trans</i> - 1 •2ClO ₄
Empirical formula	C ₅₄ H ₃₄ Cl ₈ F ₁₂ Ir ₂ N ₁₂ P ₂	C ₆₀ H ₄₅ Cl ₁₀ Ir ₂ N ₁₄ O _{8.5}	C ₆₄ H ₅₁ Cl ₁₀ Ir ₂ N ₁₆ O _{8.5}
Formula weight	1808.87	1837.0	1919.11
Temperature (K)	293(2)	296(2)	293(2)
Crystal system	Triclinic	Triclinic	Triclinic
space group	P-1	P-1	P-1
a /Å	15.504(3)	11.066(11)	16.263(3)
b /Å	16.732(3)	18.040(19)	16.337(3)
c /Å	17.196(3)	18.105(18)	17.180(3)
α /°	82.46(3)	78.90(2)	99.21(3)
β /°	65.65(3)	80.22(2)	117.64(3)
γ /°	68.98(3)	75.74(2)	103.45(3)
V/Å ³	3792.6(13)	3409.2(6)	3737.7(13)
Z	2	2	2
ρ _{calc} (g/cm ³)	1.584	1.789	1.705
μ/mm ⁻¹	3.899	4.356	3.978
R _{int}	0.0548	0.0690	0.0459
Goodness-of-fit on F ²	0.901	1.011	1.026
R ₁ ^a , wR ₂ ^b [I>2σ(I)]	0.0727, 0.1928	0.0650, 0.1562	0.0596, 0.1511
R ₁ , wR ₂ (all data)	0.1281, 0.2199	0.1294, 0.1925	0.0955, 0.1761

^a $R_1 = \sum ||F_o| - |F_c|| / \sum |F_o|$. ^b $wR_2 = \{ \sum [w(F_o^2 - F_c^2)^2] / \sum [w(F_o^2)^2] \}^{1/2}$

8. Supporting information references

- 1 M. Nonoyama, *Bull. Chem. Soc. Jpn.*, 1974, **47**, 767.
- 2 (a) F. Kong, X. Meng, R. Chu, K. Xu, B. Tang, *Chem. Commun.*, 2015, **51**, 6925;
(b) S. Mikuzami, T. Negano, Y. Urano, A. Odani, K. Kikuchi, *J. Am. Chem. Soc.*, 2002, **124**, 3920.
- 3 A. D. Becke, *J. Chem. Phys.*, 1993, **98**, 5648.
- 4 C. Lee, W. Yang, R. G. Parr, *Phys. Rev. B*, 1988, **37**, 785.
- 5 P. J. Hay, W. R. Wadt, *J. Chem. Phys.*, 1985, **82**, 270.
- 6 J. Tomasi, B. Mennucci, R. Cammi, *Chem. Rev.*, 2005, **105**, 2999.
- 7 Y. Zhao, D. G. Truhlar, *Theor. Chem. Acc.*, 2008, **120**, 215.
- 8 V. Barone, M. Cossi, *J. Phys. Chem. A*, 1998, **102**, 1995.
- 9 M. Cossi, N. Rega, G. Scalmani, V. Barone, *J. Comput. Chem.*, 2003, **24**, 669.
- 10 M. J. Frisch, G. W. Trucks, H. B. Schlegel, G. E. Scuseria, M. A. Robb, J. R. Cheeseman, G. Scalmani, V. Barone, B. Mennucci, G. A. Petersson, H. Nakatsuji, M. Caricato, X. Li, H. P. Hratchian, A. F. Izmaylov, J. Bloino, G. Zheng, J. L. Sonnenberg, M. Hada, M. Ehara, K. Toyota, R. Fukuda, J. Hasegawa, M. Ishida, T. Nakajima, Y. Honda, O. Kitao, H. Nakai, T. Vreven, J. A. Montgomery, Jr., J. E. Peralta, F. Ogliaro, M. Bearpark, J. J. Heyd, E. Brothers, K. N. Kudin, V. N. Staroverov, R. Kobayashi, J. Normand, K. Raghavachari, A. Rendell, J. C. Burant, S. S. Iyengar, J. Tomasi, M. Cossi, N. Rega, J. M. M. Millam, M. Klene, J. E. K. Knox, J. B. C. Cross, V. Bakken, C. Adamo, J. Jaramillo, R. Gomperts, R. E. Stratmann, O. Yazyev, A. J. Austin, R. Cammi, C. Pomelli, J. W. Ochterski, R. L. Martin, K. Morokuma, V. G. Zakrzewski, G. A. Voth, P. Salvador, J. J. Dannenberg, S. Dapprich, A. D. Daniels, O. Farkas, J. B. Foresman, J. V. Ortiz, J. Cioslowski and D. J. Fox, *Gaussian 09, Revision A.02*, Gaussian, Inc, Wallingford CT, 2009.